Human Molecular Genetics, 2014, Vol. 23, No. 6 **1399–1412**
doi:10.1093/hmg/ddt526
Advance Access published on October 23, 2013

Partial complex I deficiency due to the CNS conditional ablation of *Ndufa5* results in a mild chronic encephalopathy but no increase in oxidative damage

Susana Peralta[1,†], Alessandra Torraco[1,†,‡], Tina Wenz[1,¶], Sofia Garcia[1], Francisca Diaz[1] and Carlos T. Moraes[1,2,*]

[1]Departments of Neurology and [2]Cell Biology, University of Miami, Miller School of Medicine, Miami, FL, USA

Received August 6, 2013; Revised September 13, 2013; Accepted October 17, 2013

Deficiencies in the complex I (CI; NADH-ubiquinone oxidoreductase) of the respiratory chain are frequent causes of mitochondrial diseases and have been associated with other neurodegenerative disorders, such as Parkinson's disease. The NADH-ubiquinone oxidoreductase 1 alpha subcomplex subunit 5 (NDUFA5) is a nuclear-encoded structural subunit of CI, located in the peripheral arm. We inactivated *Ndufa5* in mice by the gene-trap methodology and found that this protein is required for embryonic survival. Therefore, we have created a conditional *Ndufa5* knockout (KO) allele by introducing a rescuing *Ndufa5* cDNA transgene flanked by loxP sites, which was selectively ablated in neurons by the *CaMKIIα-Cre*. At the age of 11 months, mice with a central nervous system knockout of Ndufa5 (*Ndufa5* CNS-KO) showed lethargy and loss of motor skills. In these mice cortices, the levels of NDUFA5 protein were reduced to 25% of controls. Fully assembled CI levels were also greatly reduced in cortex and CI activity in homogenates was reduced to 60% of controls. Despite the biochemical phenotype, no oxidative damage, neuronal death or gliosis were detected in the *Ndufa5* CNS-KO brain at this age. These results showed that a partial defect in CI in neurons can lead to late-onset motor phenotypes without neuronal loss or oxidative damage.

INTRODUCTION

Complex I (CI) or NADH-ubiquinone oxidoreductase is the first complex of the mitochondrial oxidative phosphorylation (OXPHOS) system that catalyzes the electron transfer from the oxidation of NADH to ubiquinone (1). The energy released from this reaction is coupled with the pumping of protons across the mitochondrial inner membrane to help generate the electrochemical gradient needed for the synthesis of ATP (2). The eukaryotic CI, with a molecular weight close to 1 MDa, consists of 45 different subunits, of which 7 are encoded by the mitochondrial DNA (mtDNA) and the remaining by the nuclear DNA (nDNA) (3,4). Of the 38 nDNA-coded subunits, 31 are considered 'supernumerary', as they are recent evolutionary additions and are believed to have regulatory functions. CI has an 'L'-shaped structure, with a hydrophobic arm embedded in the mitochondrial inner membrane and a hydrophilic peripheral arm located in the mitochondrial matrix (5,6).

Defects in CI cause a wide range of diseases, ranging from lethal infantile mitochondrial disease (i.e. Leigh syndrome) to milder ones like adult onset neurodegenerative disorders (i.e. Leber Hereditary Optic Neuropathy, LHON) (7,8). Pathogenic mutations have been described in the core subunits, including the 7 mtDNA-encoded and 7 nDNA-encoded (7,9), as well as in genes encoding for assembly factors (10–12).

Besides genetics disorders, CI defects have been observed in several neurodegenerative diseases, i.e. Huntington's and

*To whom correspondence should be addressed at: University of Miami, Miller School of Medicine, 1420 NW 9th Avenue, Room 229, Miami, FL 33136, USA. Tel: +1 305 243 5858; Fax: +1 305 243 6955; Email: cmoraes@med.miami.edu
†These authors contributed equally to this work.
‡Present address: Unit of Molecular Medicine for Neuromuscular and Neurodegenerative Diseases, Bambino Gesù Children's Hospital, IRCCS, Rome, Italy.
¶Present address: Institute for Genetics and Cluster of Excellence: Cellular Stress Responses in Aging-Associated Diseases (CECAD), University of Cologne, Zülpicher Str. 47A, 50674 Cologne, Germany and German Network for mitochondrial disorders (mitoNET).

Parkinson's disease (PD) (13) (14–16). The CI inhibitory effect of MPTP and rotenone strengthened this association in PD, as humans and animals exposed to these drugs develop Parkinsonism (17–21). However, despite the relevance of CI defects to human diseases, the patho-mechanism of CI deficiency is still poorly understood. Efforts have been undertaken in the last few years to model CI defects in mice (22). To date, mouse models for isolated CI deficiency have been reported for *Ndufs4* (23–27), *Ndufs6* (28) and *Apoptosis-Inducing Factor* (AIF) genes (29,30). Additionally, a mouse mtDNA mutant model of LHON has been recently published (31). These models have successfully recapitulated some of the symptoms found in severe early onset human diseases. However, less severe models are needed to better understand the consequences of partial CI deficiencies, particularly in the CNS.

In the present study, a neuronal-specific CI knockout (KO) mouse model was created by conditionally deleting the *Ndufa5* gene, coding for 1 of 31 supernumerary nDNA-encoded subunits. NADH-ubiquinone oxidoreductase 1 alpha subcomplex subunit 5 (NDUFA5) has a molecular mass of 13 kDa and is ubiquitously expressed in mammals. Studies performed with the bovine CI has located NDUFA5 in the peripheral arm (32); however, its specific function in CI is still unknown.

RESULTS

Generation of *Ndufa5 CNS*-KO mice

Ubiquitous *Ndufa5* KO mice were generated using gene-trap ES cell lines from the Sanger Institute Gene Trap Resource (SIGTR) following standard procedures (33). The insertion site of the gene trap was mapped onto intron 2 of the *Ndufa5* gene (Fig. 1A). Lines with germline transmission were obtained, and subsequent breeding showed that mice homozygous for the *Ndufa5 trap* were embryonic lethal, not developing beyond day E9 (Fig. 1B). To create a conditional KO mouse model with CI deficiency, a transgenic mouse expressing NDUFA5 protein ubiquitously (under the ROSA26 promoter) was created. The transgene contained the cDNA encoding for the NDUFA5 protein flanked by two loxP sites (denoted in Fig. 1C as *Ndufa5-Flx*). Mice homozygous for the disrupted allele and harboring the floxed transgene provided a conditional transgenic allele, which was first backcrossed to C57/Bl6 mice and finally crossed to a *CaMKIIa-Cre* mouse (Fig. 1D). As expected, the expression of the transgenic ROSA26-*Ndufa5-Flx* rescued the lethality of the homozygous *Ndufa5*-trap mice. Animals were obtained at the expected Mendelian ratios (data not shown). Figure 1E shows the PCR analyses of mice for the different alleles.

The *CaMKIIα* promoter starts to be expressed at birth in forebrain neurons affecting mainly the cortex and hippocampus (34). Control animals, carrying the *Ndufa5*-trap either in heterozygosis or in homozygosis, were positive for the rescuing transgene and negative for the *CaMKIIa*-Cre. We estimated the extent of the *Ndufa5*-floxed transgene ablation in the cortex over time by real time-polymerase chain reaction (RT-PCR) and found it to be markedly reduced already at 4 months of age, with no major changes in subsequent months (Fig. 1F). Likewise, the levels of NDUFA5 protein detected by western blot were highly reduced in the cortex homogenates of 4- and 11-month-old mice with a central nervous system knockout of Ndufa5 (*Ndufa5* CNS-KO) (Fig. 1G and H).

Phenotype of the CNS conditional Ndufa5 mice

Ndufa5 CNS-KO mice appeared healthy until they reached the age of 10–11 months and body weight was no different between groups (Fig. 2A). However, at this age, they became lethargic (Fig. 2B) and failed the pole descend test (Fig. 2C). In average, *Ndufa5* CNS-KO animals showed longer latency to descend the pole, indicative of loss of motor control (Fig. 2C). In addition, they clasped the hind legs when suspended by their tail. To further determine the phenotype of this motor coordination deficit, the animals were subjected to the grid and beam-walking tests. In both tasks, the *Ndufa5* CNS-KO mice showed significantly reduced motor coordination compared to control mice of the same age (Fig. 2D and E). When allowed to walk during 5 min on a grid, these KO mice manifested an increase in the percentage of 'foot errors' compared to controls (Fig. 2D). In addition, the *Ndufa5* CNS-KO mice had difficulties maintaining balance and walk on a 1 cm wide, 1 m long beam (Fig. 2E). The *Ndufa5* CNS-KO mice took almost four times longer than control mice to perform this task. In the present study, all mice were analyzed at 11 months of age, unless noted.

Ndufa5 CNS-KO mice exhibit CI deficiency in cortex

To study the effect of the *Ndufa5* deletion by *CaMKIIa-Cre*, homogenates were prepared from the cortices of *Ndufa5* CNS-KO and control mice. First, to characterize the steady-state levels of the fully assembled OXPHOS complexes, blue native (BN) gel electrophoresis experiments were carried out using different monoclonal antibodies against subunits of the respiratory complexes and a polyclonal antibody anti-NDUFA5 (Fig. 3A). We found that fully assembled CI levels were markedly reduced in the cortex of *Ndufa5* CNS-KO mice. Densitometry analysis of blots probed with an anti-NDUFA9 antibody showed that *Ndufa5* CNS-KO mice had ∼70% of reduction in assembled CI levels when compared with control values (Fig. 3B). The quantification of BN gels with anti-NDUFA5 indicated an even higher reduction (∼85%, Fig. 3B). This discrepancy may be due to either non-linearity of the western detection with different antibodies, or the presence of CI lacking NDUFA5. Controls and *Ndufa5* CNS-KO mice showed comparable steady-state levels of the fully assembled CII, CIII and CIV (Fig. 3A). The respiratory complexes were also analyzed by two dimensional-BN (2D-BN) gel electrophoresis. No CI subassembly accumulation was detected in cortices of *Ndufa5* CNS-KO mice (data not shown). Next, to determine the effect of *Ndufa5* deletion in supercomplexes, cortex homogenates were treated with a milder detergent (digitonin at a protein to detergent ratio of 1:8) and analyzed in appropriate BN gels. Besides the reduction in assembled CI levels, *Ndufa5* CNS-KO mice showed no other abnormalities, with CI present mainly in supercomplexes (analyzed with the NDUFA9 antibody, Fig. 3E). CIII was detected with anti-UQCRC2 antibody. In control animals, CIII was predominantly present in supercomplexes, just as for CI (Fig. 3E). However, the opposite pattern was detected in *Ndufa5* CNS-KO mice. The majority of CIII was detected in the band corresponding to isolated CIII (Fig. 3E). This result

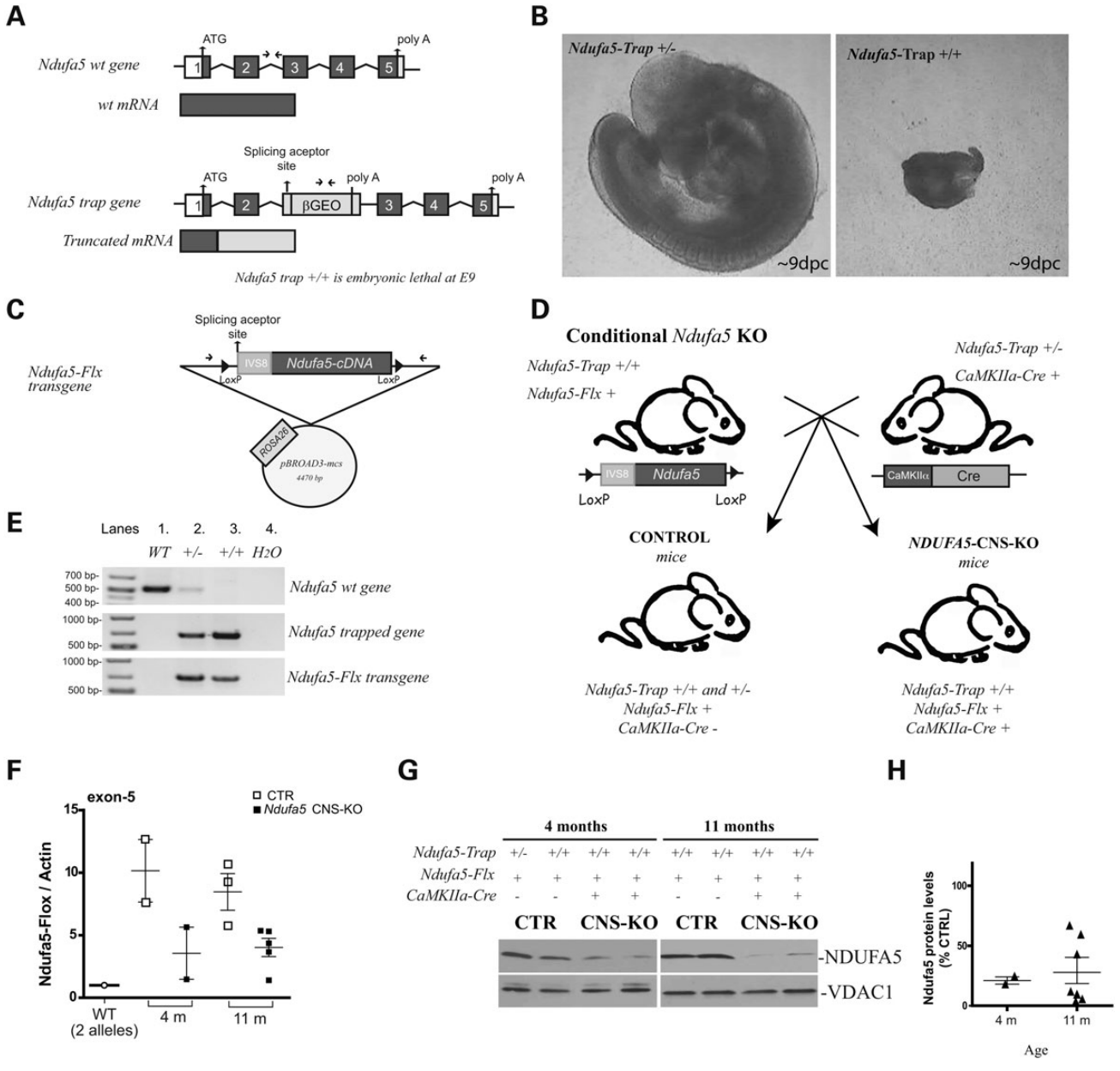

Figure 1. Creation of neuron-specific *Ndufa5* KO mice using the Cre-loxP system on a gene-trap allele. (**A**) Schematic representation of *Ndufa5* gene (NCBI gene ID: 68202) and insertion of the gene-trap vector into intron 2 of *Ndufa5* gene. Exons are indicated by numbered boxes and introns by lines. Translated sequences are shown in gray and untranslated in white. βGEO, β-galactosidase–neomycin resistance cassette. (**B**) Representative light microscopy picture of E9 embryos heterozygous (left) and homozygous (right) for *Ndufa5*-trapped alleles. (**C**) Scheme of the construct used to generate transgenic mice expressing a conditional *Ndufa5* allele. (**D**) Crossing scheme used to generate a neuron-specific *Ndufa5* KO mouse model, named mice with a central nervous system knockout of Ndufa5 (*Ndufa5* CNS-KO). *Ndufa5* KO mice are homozygous for the *Ndufa5*-trapped gene, positive for the rescuing floxed *Ndufa5* and for the *CaMKIIα-Cre* transgenes. *CaMKIIa*: Ca^{2+}/calmodulin-dependent protein kinase II type α. (**E**) Molecular confirmation of the gene-trap insertion. PCR products from genomic DNA of mouse tails amplified with primers showed in A and C (arrows). Upper panel: wild-type gene. Middle panel: *Ndufa5*-trapped gene. Bottom panel: rescue construct. (**F**) Quantification of *Ndufa5*-floxed transgene by real-time PCR. Exon 5 from genomic DNA isolated from cortex was quantified. Two copies of the gene observed in wild-type mice were given a value of '1'. Open circles represent wild-type values. Open squares represent transgenic control values. Filled squares represent the *Ndufa5* CNS-KO. Values were calculated by the $\Delta\Delta C_t$ method. (**G**) Western blot from cortex homogenates of 4- and 11-month-old control and *Ndufa5* CNS-KO mice probed with NDUFA5 and VDAC-1 antibodies. (**H**) Quantification of NDUFA5 levels showed a reduction in cortex homogenates *Ndufa5* CNS-KO mice.

can be explained by the reduction in CI levels seen in *Ndufa5* CNS-KO (Fig. 3A and E).

The steady-state levels of NDUFA5 protein and several subunits of CI were also analyzed by sodium dodecyl sulfate (SDS)–polyacrylamide gel electrophoresis (PAGE). Figure 3C shows a markedly decrease in the levels of NDUFA5 protein in the cortex homogenates of *Ndufa5* CNS-KO mice. NDUFA9, NDUFS3, NDUFS4 and NDUFB8 CI subunits were also significantly decreased in *Ndufa5* CNS-KO mice (Fig. 3C and F). Nevertheless, the steady-state levels of SDHB (Succinate Dehydrogenase subunit B, complex II), UQCRC2 (core 2 subunit of CIII), cytochrome c, COXI (CIV subunit) as well as ATPaseα and

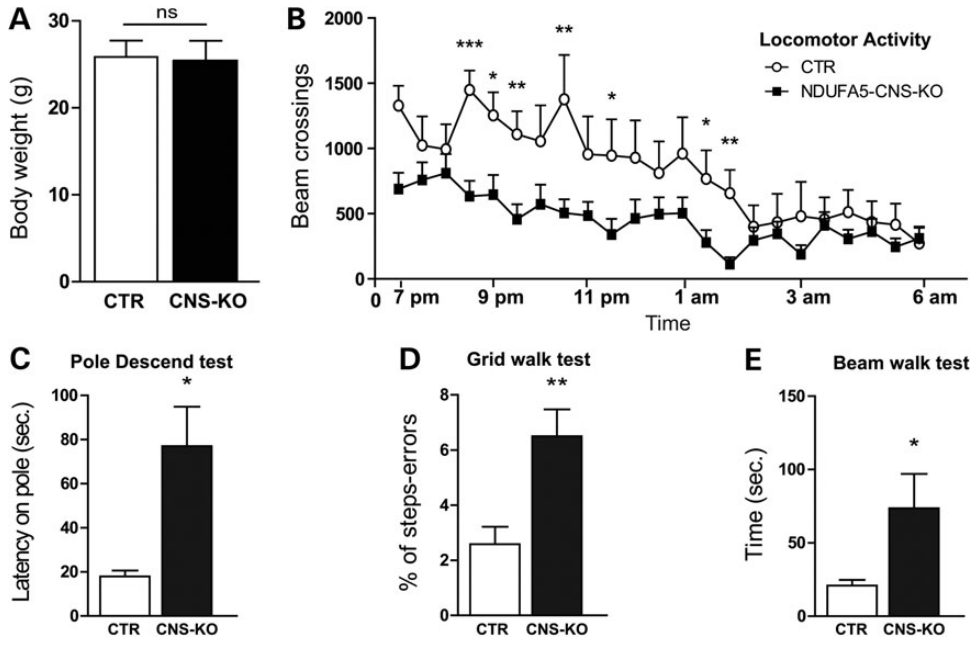

Figure 2. Phenotype of *Ndufa5* CNS-KO mice. (**A**) Comparison between body weight of control and 11-month-old *Ndufa5* CNS-KO mice; $n = 6/7$; values represent mean ± SEM. (**B**) Activity cage of 11-month-old control and *Ndufa5* CNS-KO mice. Open circles, control animals ($n = 7$) and closed squares, CNS-KO animals ($n = 8$). (**C**) Pole descend test expressed as latency on pole (time in seconds that the animal employs to descend the pole). KO animals employed 76.97 ± 17.91 s to descend the pole, whereas control animals of the same age descended in 17.93 ± 2.701 s on average; *t*-test $^{*}P = 0.0197$, $n = 7$ each group. (**D**) The grid test shows the % of steps errors done during 5 min of undisturbed walking in a grid. *Ndufa5* KO animals failed in 6.50 ± 0.97% of the total number of steps taken while the % of error developed by control animals was 2.583 ± 0.6% ($n = 7$, *t*-test, $^{**}P = 0.0056$). (**E**) Elevated beam-walking test. The time they spend to go over a 1 m length, 1 cm wide beam is measured. Control 20.9 ± 3.9 s versus *Ndufa5* CNS-KO 73.6 ± 23.4 s. Values are mean ± SEM. Data were analyzed using Student's two-tailed *t*-test, $^{*}P < 0.05$, $^{**}P < 0.01$ and $^{***}P < 0.001$.

ATPaseβ (complex V subunits) remained unchanged in *Ndufa5* CNS-KO mice (Fig. 3D and F).

To determine the effect of *Ndufa5* deletion on the function of the respiratory complexes, enzymatic activities were measured spectrophotometrically in cortex homogenates. Figure 4 shows the enzymatic activity obtained for mitochondrial CI, CII, CIII and CIV in *Ndufa5* CNS-KO mice. NADH-Coenzyme Q (CoQ) oxidoreductase (CI) activity was reduced in KO cortex homogenates by ∼40%. On the other hand, succinate decylubiquinone 2,6-dichlorophenol-indophenol reductase (CII), ubiquinol cytochrome c reductase (CIII) and cytochrome c oxidase (CIV) activities remained unchanged in the *Ndufa5* CNS-KO mice (Fig. 4A). These results are in concordance with the results obtained in the BN gels (Fig. 3A), indicating an isolated CI defect. No difference was observed between control and *Ndufa5* CNS-KO mice in cortex citrate synthase activity (Fig. 4B).

Mitochondrial OXPHOS deficiency impairs pyruvate oxidation in the mitochondria, which is then converted into lactate. This lactate could accumulate in the tissues and bloodstream (35). To analyze if the partial CI defect observed in the cortex of *Ndufa5* CNS-KO mice led to lactic acidosis, we measured lactate concentration in serum. Although there was a trend towards higher lactate concentration in the blood of *Ndufa5* CNS-KO, it did not reach statistical significance (Fig. 4C).

Potential compensatory mechanisms in Ndufa5 CNS-KO mice

The catabolism of fatty acids in mitochondria has a few metabolic pathways that can generate ATP independently of OXPHOS. Although these pathways may not be very active in normal CNS physiological conditions, they could be upregulated when there is energy shortage. Therefore, we characterized whether fatty acid metabolism was affected by the partial CI deficiency.

The activities of mitochondrial enzymes involved in β-oxidation of fatty acids were measured in cortex homogenates (Fig. 4D). *Ndufa5* CNS-KO cortices did not reveal differences in the activity of 3-L-hydroxyacyl-CoA dehydrogenase and palmitoyl-CoA dehydrogenase (Fig. 4D). In addition, the levels of transcripts coding for the plasma membrane transporter of fatty acids (CD36/FAT), the peroxisome enzyme (acyl-CoA oxidase) and several acyl-CoA dehydrogenases were not altered in KO cortices when measured by RT-PCR (Supplementary Material, Fig. S1). Western blots for medium-chain acyl-CoA dehydrogenase (MCAD), one of the enzymes involved in mitochondrial fatty acid β-oxidation, showed a trend, but no significant differences, in the *Ndufa5* CNS-KO (Fig. 4E).

Because fatty acid metabolism generates reduced equivalents that can be oxidized via CoQ10 through the electron transfer flavoprotein dehydrogenase complex (ETF-A-B and ETFdh) (36), protein levels of subunit A (ETFA) were measured. The

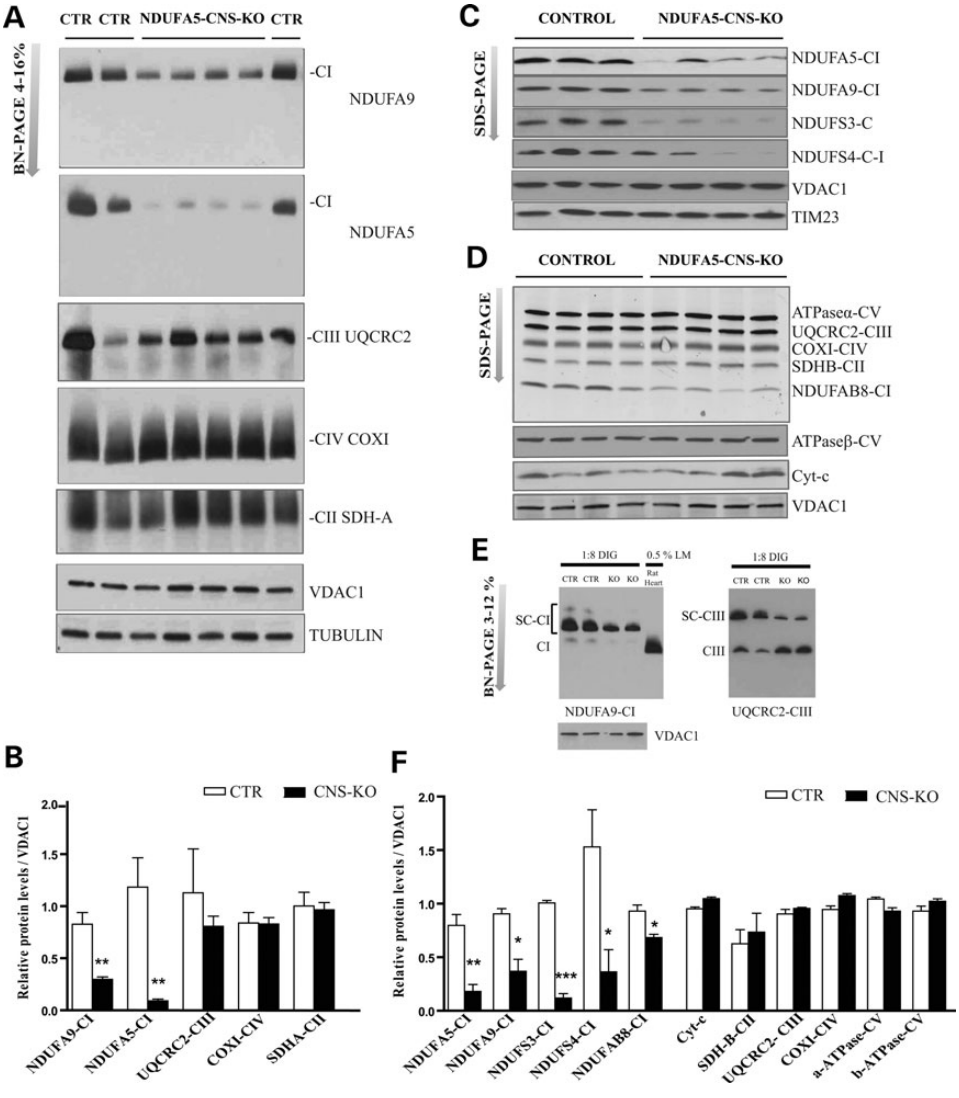

Figure 3. *Ndufa5* CNS-KO mice showed an isolated defect of CI in cortex. (**A**) Steady-state levels of respiratory complexes in cortex homogenates from 11-month-old control and *Ndufa5* CNS-KO mice. Respiratory complexes in cortex (20 μg) from control and KO mice were separated by BN-PAGE (4–16% gels, $n = 4$ each group). (**B**) Quantification of BN-PAGE in (A) showing complexes levels normalized to voltage-dependent anion channel 1 and to control animals. *Ndufa5* CNS-KO showed a reduction in assembled CI (*t-test* $P = 0.0029$ for NDUFA9 and for NDUFA5 *t-test* $P = 0.0056$). (**C** and **D**) Western blots showing the levels of NDUFA5 and mitochondrial proteins in the cortex homogenates from 11-month-old control and *Ndufa5* CNS-KO mice ($n = 4$ each group). NDUFA5 levels in KO were reduced to 20% versus control (*t-test,* $^{**}P = 0.003$). (**E**) Steady-state levels of respiratory supercomplexes in cortex. (**F**) Quantification of SDS–PAGE in (C and D). Values represent mean ± SEM. Data were analyzed using Student's two-tailed *t*-test, $^{*}P < 0.05$, $^{**}P < 0.01$ and $^{***}P < 0.001$.

steady-state levels of ETFA were significantly increased in the cortex homogenates of *Ndufa5* CNS-KO (Fig. 4E, 50% higher), suggesting a potential compensatory mechanism, which could help explain the mild phenotype.

Ketone bodies have been shown to improve oxidative phosphorylation, via a mechanism dependent on mitochondrial CII, in a drug-induced (MPTP) CI-deficient mouse model (37). Thus, to further characterize the effect of partial CI deficiency in the metabolic pathways in brain, the levels of two enzymes implicated in the metabolism of ketone bodies were examined by the western blot (Fig. 4F). The levels of succinyl-CoA-3-ketoacid CoA transferase (SCOT), which converts acetocetate to acetoacetyl-CoA, were not significantly different between KO and controls (Fig. 4F). However, the levels of the mitochondrial acetyl-CoA acetyl transferase 1 (ACAT-1), were elevated in *Ndufa5* CNS-KO cortex (Fig. 4F). This increase may enhance ketone bodies metabolism in the *Ndufa5* CNS-KO to counteract the CI defect.

Histological analysis of Ndufa5 CNS-KO mice cortex did not show morphological changes

The light and confocal microscopy study of sections from the cerebrum and cerebellum did not reveal major differences between 11-month-old *Ndufa5* CNS-KO and control (Fig. 5) mice. Figure 5A shows sagittal sections of the motor cortex of control and KO animals stained with hematoxylin and eosin (H&E). No differences in the cortical thickness or general structure of the cortex between groups were found. Likewise, histological comparisons between hippocampus and cerebellum

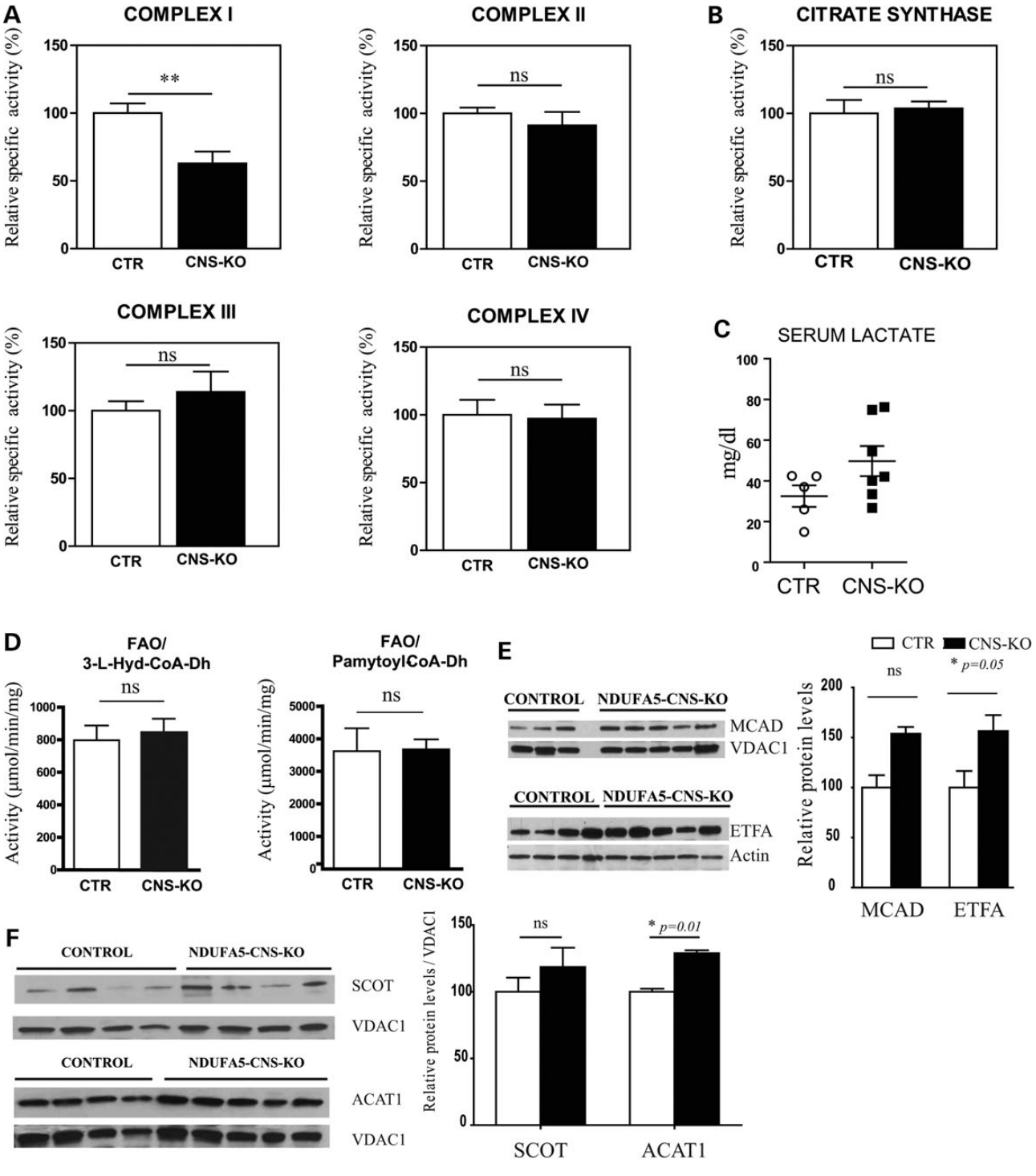

Figure 4. Biochemical characterization of cortex from 11-month-old *Ndufa5* CNS-KO mice. (**A**) and (**B**) Mitochondrial enzyme and citrate synthase activities in cortex of control and *Ndufa5* CNS-KO mice were determined spectrophotometrically and expressed as the percentage of mean values obtained from control animals. CI: NADH-Coenzyme Q oxidoreductase activity; CII: succinate decylubiquinone 2,6-dichlorophenol-indophenol reductase; CIII: ubiquinol cytochrome c reductase and CIV: cytochrome c oxidase. $n = 7$/controls and $n = 8$/*Ndufa5* CNS-KO mice. CI activity *t-test*, $^{**}P < 0.01$. (**C**) Lactate levels detected in the blood serum from control and *Ndufa5* CNS-KO mice. $n = 5$/control and $n = 7$/KO. (**D**) L-3-hydroxyacyl-CoA dehydrogenase and palmitoyl-CoA dehydrogenase enzymatic activities of control and *Ndufa5* CNS-KO mice. Mean ± SEM values are represented ($n = 4$ in each group); FAO, fatty acid oxidation. (**E**) Western blots and quantification of MCAD (FAO-related enzyme) and of electron transfer flavoprotein subunit A (ETFA) mitochondrial proteins in cortex homogenates from control and *Ndufa5* CNS-KO. ETFA levels in KO were 156.4 ± 15.9% versus 100.0 ± 16.5 in control (*t-test*, $^{*}P = 0.05$). (**F**) SCOT and ACAT-1 were determined by the western blot and were quantified by densitometry. Values represent mean ± SEM.

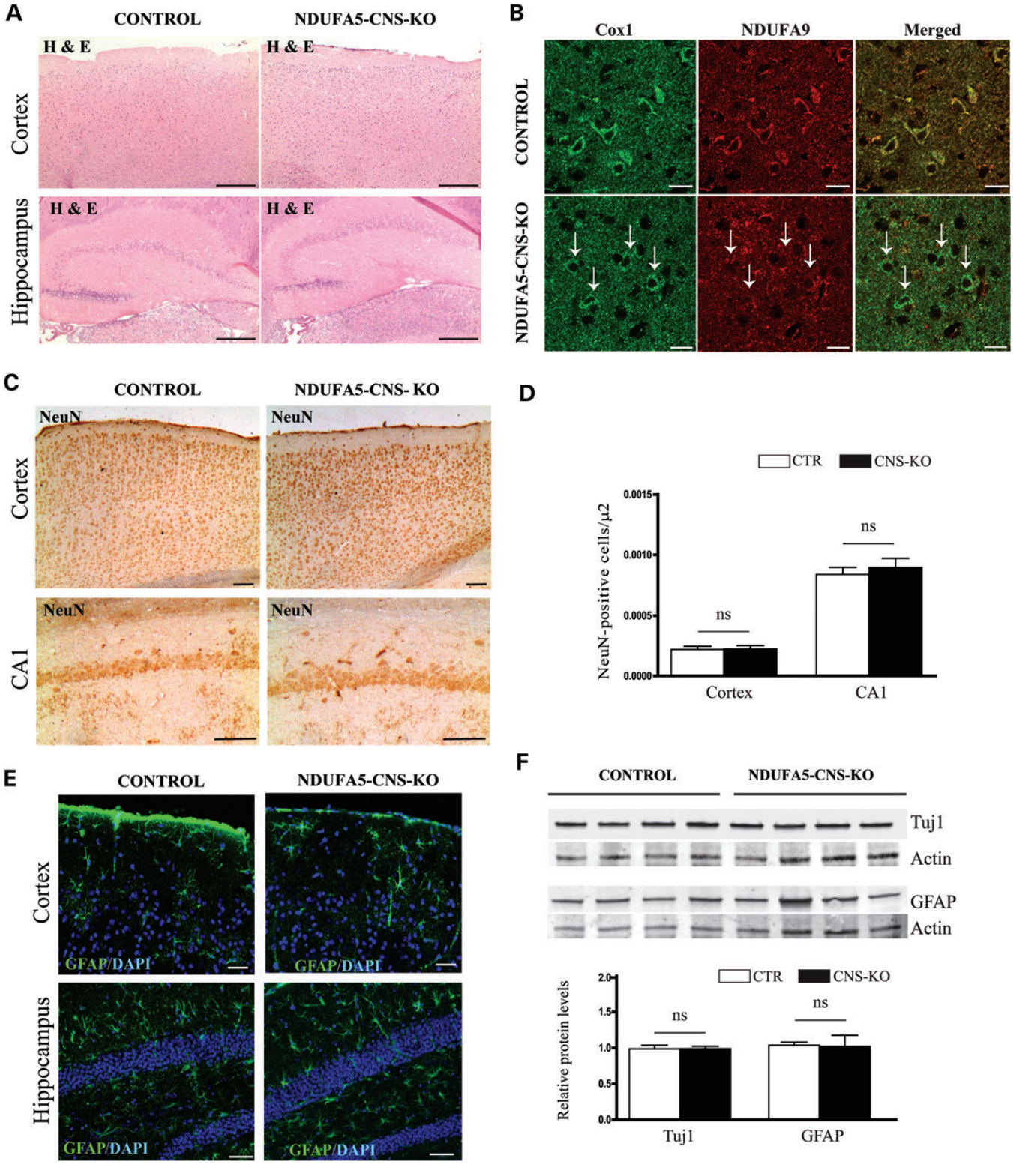

Figure 5. Histological comparisons between cortex and hippocampus from control and *Ndufa5* CNS-KO show no pathological features in 11-month-old mice. (**A**) H&E analyses of cortex, and hippocampus from control and *Ndufa5* CNS-KO mice. Bars = 200 μm. (**B**) Immunostaing of NDUFA9 and COX1 in cortex. White arrows indicate neurons that are positive for COX1 and deficient in NDUFA9. Bars = 20 μm. (**C**) Representative sections of motor cortex and hippocampus region CA1 immunostained with the neuron-specific antibody NeuN, $n = 3$ of each group. Bars = 100 μm and quantified in panel (**D**). (**E**) Confocal microscopy of section from cortices and hippocampus immunostained with the glial-specific antibodies GFAP. Bars = 50 μm. (**F**) Western analyses of cortex homogenates from control and *Ndufa5* CNS-KO mice probed with the neuronal-specific antibody Tuj1 and the glial marker GFAP. Actin was used as an internal standard. The lower part of F shows the quantification of the western blots normalized to actin, and normalized to the average of ratios of control group ($n = 4$ per group). NeuN: anti-neuronal nuclear marker NeuN; Tuj1: anti-neuron-specific class III beta-tubulin; GFAP: anti-glial fibrillary acidic protein antibody.

indicated no pathological features in *Ndufa5* CNS-KO (Fig. 5A and Supplementary Material, Fig. S2). To address the CI deficiency in the neurons of the *Ndufa5* CNS-KO mice, brain sections were immunostained with the anti-NDUFA9 antibody, and with the anti-COXI (CIV subunit) antibody as a mitochondrial control (Fig. 5B). White arrows in the confocal microscopy panels of Figure 5B indicate CI-deficient neurons.

To study for potential neuronal loss, immunohistochemistry with the neuronal marker NeuN was performed on sagittal sections of *Ndufa5* CNS-KO and control mice. Representative sections of the motor cortex and hippocampus region CA1 are shown in Figure 5C. Quantification of the number of NeuN-positive cells in those regions showed no differences between groups (Fig. 5D). Confocal microscopy showed no differences in NeuN-positive cells in neither cortex, nor hippocampus, nor cerebellum between groups (Supplementary Material, Figs S2 and S3). Furthermore, because glial reactivity is a common feature accompanying neuronal loss, predominantly in the early stages, we stained brain sections for the astroglial marker glial fibrillary acidic protein (GFAP) and for the microglia-specific protein Iba1. No differences in GFAP and in Iba1 signal were observed between KO and control specimens (Fig. 5E and Supplementary Material, Fig. S3). Thus, neither neuronal loss, nor gliosis, was observed in the cortex and hippocampus sections of the *Ndufa5* CNS-KO mice. We quantified the levels of some of these markers by the western blot of *Ndufa5* CNS-KO mice cortex homogenates (Fig. 5F). The quantification of neuronal class III β-Tubulin (Tuj1) and GFAP by western blots showed no differences in their levels between groups (Fig. 5F).

Ndufa5 CNS-KO cortices do not show oxidative damage

CI deficiency has been correlated with an increase in reactive oxygen species (ROS) in fibroblasts of patients (38) as well as in the Harlequin and *Nestin-Cre-Ndufs4* mouse models (26,29,30). To detect whether, in our model, the partial CI deficiency induced by the reduction of NDUFA5 protein caused oxidative damage, we examined the oxidation levels of the nucleic acids in brain sections and the oxidation of lipids and proteins in cortices homogenates (Fig. 6). To investigate nucleic acid oxidation, 8-hydroxy-deoxyguanosine/8-hydroxyguanosine (8-OHdG/8-OHG) immuno staining was performed in brain sections (Fig. 6A). 8-OHdG and 8-OHG are products of DNA and RNA oxidation, respectively (39). No differences in the staining were found between groups (Fig. 6A). To detect lipid peroxidation, 4-hydroxy-2-nonenal (4-HNE) protein adducts were evaluated by the western blot. 4-HNE is a major product of endogenous lipid peroxidation and its presence is considered a reliable marker of increased cellular oxidative stress. In addition, no significant changes in 4-HNE adduct content were detected (Fig. 6B and C).

Oxidative reactions cause carbonyl groups to be introduced into proteins. The overall levels of protein carbonyl groups were similar between control and *Ndufa5* CNS-KO (Fig. 6D). In addition, the levels of enzymes responsible for detoxifying superoxide radicals: Cu/Zn−superoxide dismutase or SOD1, and SOD2 were also measured. In agreement to the previous results, no significant differences were observed in the cortex of *Ndufa5* CNS-KO (Fig. 6E and F). All together, these results indicate that the partial CI deficiency in the *Ndufa5* CNS-KO brain does not lead to significant oxidative stress.

DISCUSSION

Ablation of the Ndufa5 gene in CaMKIIa-positive neurons causes a mild encephalopathy

Defects in CI have been associated with genetic disorders and neurodegenerative conditions, notably PD. Still, very few models of CI deficiency have been studied in mammals to date, and almost all associated with early death. We have used the *CaMKIIa-Cre* to drive the postnatal deletion of a KO-rescuing *Ndufa5*-floxed transgene in forebrain neurons, generating a milder phenotype.

Although the specific function of NDUFA5 subunit in CI remains unknown, our data showed it to be required for CI assembly/stability in mammals. We have detected a partial decrease in CI levels and activity at 11 months in our CNS model. The quantification of BN gels indicated a 70% reduction in assembled CI containing NDUFA9 subunit versus a 85% reduction in assembled CI containing NDUFA5. This result suggests the presence of a percentage (15%) of assembled CI that does not contain NDUFA5 subunit in this model. Although this would suggest that NDUFA5 subunit is not essential for the assembly process, this difference could be explained by the non-linearity of western blot quantitations using different antibodies. Therefore, at this point, we do not have strong evidence that a stable CI subassembly can exist without NDUFA5.

Interestingly, although the steady-state levels of assembled CI were highly decreased (70−85% reduction), the enzymatic activity of CI showed a 40% reduction in the CNS-KO. This discrepancy may be due to a reduced stability of the CI in the absence of the NDUFA5 subunit in the BN-PAGE assay. In addition, the enzymatic assays were performed under optimal conditions of electron donor and acceptor, reflecting maximal activities. Although there was a decrease in the levels of supercomplexes containing CI in the KO brains, essentially all the residual CI was found in supercomplexes that are believed to optimize electron transfer (40,41). The CI deficiency correlated with a mild motor phenotype, including decreased motor skills and ambulatory activity reduced at the same age.

To date, the best-studied model of CI deficiency is a ubiquitous KO of *Ndufs4* gene, which, in contrast to our model, develops a severe ataxic encephalopathy with death ∼50 days after birth (24). Deleting the gene only in the brain, driven by the *Nestin-Cre* line, caused a similarly severe phenotype (26). The olfactory bulb and vestibular nucleus of the brainstem, and the posterior lobules of the cerebellar vermis, were particularly affected in that model. Those regions showed loss of neurons as well as severe glial activation. There are differences between the models that could explain the milder phenotype of our model, including the fact that we used a *CaMKIIa-Cre* (*CaMKIIa* neuron specific, 33), whereas Quintana and colleagues used a *Nestin*-Cre (expressed both in neurons and glia). Another cause that may contribute to the severe phenotype of the *Ndufs4*-KO model is its absence during development, as Nestin-driven expression is early embryonic in neuronal precursors. In contrast, *CaMKIIa*-driven expression is postnatal (34). Thus, these results suggest that a functional CI during the

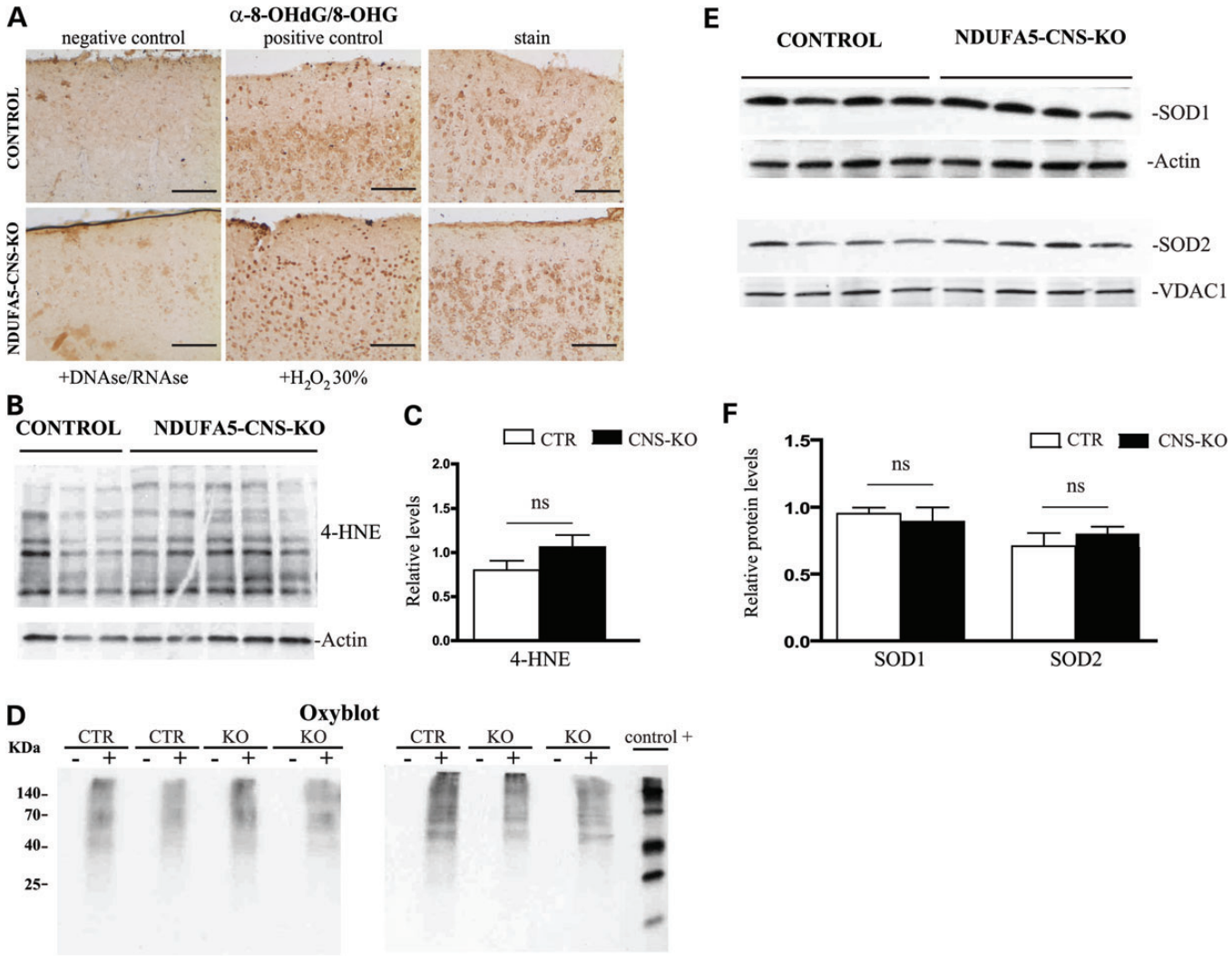

Figure 6. Characterization of oxidative stress markers in *Ndufa5* CNS-KO. (**A**) Determination of oxidative damage to nucleic acids. Brain sections from 11-month-old control (upper) and from *Ndufa5* CNS-KO (lower) were stained with anti-OHG antibody. For a negative control, brain sections were pre-treated with Dnase/Rnase. For a positive control, brain sections were pre-treated with 30% H_2O_2. Representative sections are showed from $n = 5$ of each group. Bars = 100 μm. (**B**) Western analyses of cortex homogenates (20 μg) from 11-month-old control and *Ndufa5* CNS-KO mice were incubated with an antibody against 4-HNE adducts. (**C**) Quantification of the bands and normalized to actin and to the control group. Control 0.800 ± 0.1079 ($n = 3$) and KO 1.062 ± 0.1374 ($n = 5$). ns, not significant. (**D**) Oxyblot: immunoblot detection of carbonyl residues on proteins (20 μg) from cortex homogenates. No differences were found between control and KO group. (**E**) SDS–PAGE of cortex homogenates (20 μg) from control and *Ndufa5* CNS-KO blotted against SOD1 and SOD2. The total amount of SOD1 and SOD2 was quantified and normalized by the amount of actin and VDAC1, respectively, and normalized to the average of ratios of control group ($n = 4$ per group). Quantification of the blots is shown in (**F**). Values were given as mean ± SEM. Data were analyzed using Student's two-tailed *t*-test, statistical significance when $P < 0.05$.

development of the CNS is required for neuronal survival. On the other hand, postnatal neurons would tolerate a better CI deficiency. Accordingly, a milder phenotype was observed when *Ndufs4* gene was inactivated ubiquitously but only in the adult mice via a tamoxifen-inducible system (26).

Moreover, recent studies have revealed that the deletion of *Ndufs4* in the vestibular nucleus resulted in respiratory failure and contributed to the lethality of the *Ndufs4*-KO mice (27).

However, using the same *CaMKIIa-Cre*, we found that deleting a gene required for CIV assembly (COX10) a more severe defect was observed, with overt onset at 3–4 months (42,43). Similarly, deletion of the catalytic subunit of CIII (Rieske iron–sulfur protein), using the *CaMKIIa* promoter, induced a more severe phenotype in mice, where animals die at the age of 3.5 months (42). Molecular or cellular compensatory mechanisms might reduce the impact of the *Ndufa5* ablation in neurons. Our data indicate that the milder phenotype observed could be related to an increased electron transfer through the Electron-transferring flavoprotein (ETF) system. ETF is involved in the oxidation of fatty acids, donating electrons directly to CoQ10, bypassing CI and CII, which would help maintain a membrane potential by CIII and CIV (36,44). In fact, we did detect an increase in the levels of ETFA subunit of the heterotrimeric enzyme.

In addition, we found that ketone bodies metabolism may also be part of this compensatory mechanism. Brain actively metabolizes ketone bodies to produce energy and for biosynthetic processes in periods of energy shortage (45,46). The ACAT1

enzyme is a mitochondrial ACAT involved in the regulation of ketogenesis (47). It catalyzes the interconversion of one molecule of acetoacetyl-CoA into two molecules of acetyl-CoA. Thus, in our model, the CI deficiency may lead to increase in ACAT1, increasing the availability of acetyl-CoA molecules that could enter the Tricarboxylic acid (TCA) cycle, generating succinate that could feed the OXPHOS system through CII. The proposed mechanism is supported by studies, showing that β-hydroxybutyrate infusion in a Parkinson mouse model rescues OXPHOS function through a mechanism dependent on CII (37). Moreover, ketogenic diet has been shown to induce a coordinated upregulation of mitochondrial genes involved in energy metabolism, and to stimulate mitochondrial biogenesis (48). Indeed, ketogenic diet slows down the progression of the myopathy of mitochondrial origin in the 'deletor' mouse (49) and reduces the pathology in a mouse model of Alzheimer disease by sustained mitochondrial energetic function (50). However, the ability of the ketone bodies to increase oxidative phosphorylation in our model, and in this sense contribute to the mild phenotype of the *Ndufa5* CNS-KO, remains to be elucidated. The TCA cycle is likely to be slowed down by a reduction in NAD^+. However, in the liver, ACAT1 has been shown to carry out a reverse reaction, which is the first step in building new ketone bodies (51). Moreover, astrocytes produce large amounts of ketone bodies (52,53). Yet another possible explanation for the increase ACAT1 levels observed is that as excessive acetyl-CoA that cannot enter the Krebs cycle will have to be eliminated by forming ketones, which may be used in biosynthetic processes (54).

The TCA cycle not only provides reducing equivalents for the OXPHOS system, but also generates high-energy phosphates (ATP/GTP) (55). The product of the α-ketoglutarate dehydrogenase (KGDHC) enzyme, succinyl-CoA, is the substrate for 'substrate-level phosphorylation' of ADP performed by the enzyme succinyl-CoA synthetase (SCS). SCS is the only enzyme capable of generating ATP in the absence of a proton motive force in the mitochondrial inner membrane, potentially playing a role in maintaining matrix ATP levels under energy-deficient conditions, such as transient hypoxia (56). Thus, this mechanism could also contribute to counteract the CI deficit in our model.

Therefore, we suggest that the relatively mild phenotype and the late onset we observed is a consequence of at least two main compensatory mechanisms: (i) increased electron transfer via the electron transfer flavoprotein dehydrogenase to CoQ10 and (ii) physiological adaptations to a ketogenic environment. A mild CI defect may have allowed time for such adaptation.

Partial CI defect in the CNS was not associated with increased oxidative damage

A large body of work *ex vivo* has shown that inhibition of CI with drugs leads to an increase in oxidative damage, mostly because of superoxide formed at the level of CI (57–59). However, we have found no oxidative damage in the brain of 11-month-old *Ndufa5* CNS-KO. Because in our model the levels of CI are highly reduced, the formation of ROS may also decrease. In agreement, we have found genetic defects that decrease the levels of OXPHOS components and did not increase oxidative damage. This was found not only in the present CI defect model, but also in mouse models of CNS CIV deficiency (42,43) and mtDNA depletion (60). Likewise, the mutator mouse, which accumulates mtDNA mutations, also showed no increase in ROS damage (61,62) and in some tissues, such as skeletal muscle, there were actually decreases in oxidative damage (63). Also in patients, the lack of NDUFS4 and the complete absence of assembled CI were not paralleled by an increase in ROS production (64). Moreover, inhibition of CI assembly by knockdown of NDUFS3 subunit or the CI assembly factor NDUFAF1 reduced the ROS production *ex vivo* (65,66). In contrast, Quintana and colleagues found increased protein carbonylation in the *Ndufs4*-KO mice, but this model showed severe astrogliosis, increased microglia and inflammation at the time points analyzed (26).

We did find increased oxidative damage in the piriform and somatosensory cortices in a mouse model of CIII defect in the CNS (*CaMKIIa-Cre* deletion of the Rieske iron–sulfur protein of CIII) (42). It is clear that the potential increase in ROS depends on the site and type of the OXPHOS defect. However, in most genetic cases, where the steady-state levels of complexes are reduced, it appears that there is no increase in ROS production or oxidative damage (67).

In summary, we developed a novel model of CI deficiency in the CNS presenting with a late-onset phenotype, which may in some ways mimic the age-related CI decrease observed in several neurodegenerative diseases (13,14).

The mild presentation, compared with defects in other respiratory complexes, may be due to increased electron transfer through the ETF system and physiological adaptations in response to a more ketogenic environment. Oxidative stress was not observed in affected brain regions, providing evidence that genetic defects affecting the CI of the respiratory chain do not result in increased ROS damage. This model will be very useful in analyzing the role of partial CI deficiency in late-onset neurodegenerative conditions.

MATERIALS AND METHODS

Generation of Ndufa5 KO mice

A *Ndufa5* gene-trap ES cell line from the SIGTR (SIGTR-clone RRK279) was fused to C57/B6 blastocyst and five chimeras were generated. After germline transmission, animals carrying an allele of the *Ndufa5* gene KO were detected by PCR. Homozygous *Ndufa5* KO mice display embryonic lethality at day E9. To rescue the lethality, the full length *Ndufa5* cDNA sequence (351 bp), flanked by the LoxP sites, was subcloned in TOPO TA vector (Invitrogen) in *Bgl*II/*Xba*I sites, and subsequently transferred to the pBROAD3-mcs v02 plasmid (Invitrogen), in *Age*I/*Hind*III sites, under the ubiquitous mouse ROSA26 promoter. Microinjection of this construct into B6/SJLF1 fertilized oocytes was performed by the transgenic core facility of the University of Miami. Those transgenic mice were subsequently crossed with the mice heterozygous for the *Ndufa5* gene trap. To KO specifically the *Ndufa5* gene in the central nervous system, the double trap and transgenic mice were mated with the *CaMKIIa*-Cre transgenic mice kindly supplied by Dr Scott Zeitlin (University of Virginia). Animals for this study were obtained following the scheme described in Figure 1E. Genetic contributions in controls and *Ndufa5* CNS-KO mice were mostly from a 129 strain, but also contained smaller percentages

of genes originating from SJL and C57/BL6 backgrounds. Controls and conditional KO mice were obtained from the same litters. The presence of the transgenes and trap was detected by PCR using the following pairs of primers. For the *Ndufa5* gene trap, forward primer used was 5′-TTATCGATGAGCGTGG TGGTTATGC-3′ and reverse primer was 5′-GCGCGTACAT CGGGCAAATAATATC-3′. For the *Ndufa5* wild-type gene, forward primer used was 5′-GATGCATTCGGTCTCATCCT-3′ and reverse was 5′-AGATCCCACCTTTGCCTTCT. For the *Ndufa5*-floxed transgene, forward primer used was 5′-CCTG ACAGGTGTGAAACAGGA-3′ and reverse was 5′-AGAAA TTGGACAGCAAGAAAG-3′. For the *CaMKIIa-Cre* transgene, forward primer used was 5′-GCGGTCTGGCAGTAAA AACTATC-3′ and reverse was 5′-GTGAAACAGCATTGCT GTCACTT-3′. The gene ID for *Ndufa5* is 68202.

All mice procedures were performed according to a protocol approved by the University of Miami Institutional Animal Care and Use Committee. Mice were housed in a virus–antigen-free facility in a 12-h light/dark cycle at room temperature and fed *ad libitum* with a standard rodent diet.

Quantitative PCR of genomic DNA

Genomic DNA was extracted from cortex using standard phenol/chloroform extraction. To quantify the deletion of the *Ndufa5*-floxed transgene (rescue transgene) in KO animals, 50 ng of genomic DNA was amplified using specific primers for *Ndufa5* gene (exon 3 and exon 5) in a 20 μl reaction mixture using Sso Advanced SYBR Green (Bio-Rad), following PCR conditions stipulated by the manufacturer in a CFX96 real-time PCR system (Bio-Rad). Standard curves were obtained using genomic DNA from control, N*dufa5* CNS-KO and wild-type mice for *Ndufa5* gene. *Ndufa5*-floxed transgene amounts were quantified using the $\Delta\Delta C_t$ method and normalized to the *Ndufa5* wild-type mice (two copies of the gene). Values were normalized to actin.

(i) *Ndufa5*-exon 5 (forward): 5′ GCTGAAAAAGAACTA AGTCTGGC 3′
(ii) *Ndufa5*-exon 5 (reverse): 5′ CATATTGGCCACTTCC ACTG 3′
(iii) β-actin (forward): 5′ GCGCAAGTACTCTGTGTGGA 3′
(iv) β-actin (reverse): 5′ CATCGTACTCCTGCTTGCTG 3′

Behavioral test

Activity cage test

Locomotor activity was measured as laser-beam breaks that occur in a locomotor chamber (Columbus Instruments), during 12 h period in their dark cycle. Animals were housed individually in a novel cage environment 30 min prior to their dark cycle and monitored undisturbed ($n = 7$ for control and $n = 8$ for *Ndufa5* CNS-KO group). To test motor coordination in *Ndufa5* CNS-KO mice ($n = 7$) and their control counterparts ($n = 7$) of 10–11 months, we have used the following tests: pole descend, beam-walking and grid-walking tests.

Pole descend test

Animals were hung upright on a vertical (8 mm diameter; 55 mm length) pole and were given 3 min to change orientation to descend. Animals were given three trials with an average taken of the latency to descend to the base. Failure to descend or fall from the pole was given a maximum time of 3 min.

Grid test

Animals were placed on a grid (30 cm width/30 cm length) and allowed to walk during 5 min while their spontaneous movement was recorded. Subsequently, the videos were analyzed and the steps errors were counted. Steps errors are defined as the times that any foot goes inside the holes of the grid. The steps errors are referred to the total number of steps given for the animal during 5 min and expressed as %.

Beam-walking test

Animals were placed on the far right of an elevated beam of 1.7 cm and motivated to walk through the 1 m distance of the beam. Animals were given three trials to traverse the beam with an average taken of the time to go over the 1 m. Animals were allowed to rest 15 min between each run.

BN-PAGE and SDS–PAGE

To identify and estimate the levels of individual respiratory complexes, cortex homogenates were treated with 1% lauryl maltoside (Sigma) and separated by BN-PAGE in 4–16% acrylamide gradient gels (Invitrogen) (68,69). For western blot analysis, 20 μg of proteins were separated by PAGE, transferred onto a polyvinylidene difluoride (PVDF) membrane (Bio-Rad), and incubated sequentially with antibodies against several subunits of the different mitochondrial respiratory complexes.

For supercomplex analyses, cortex homogenates were treated with digitonin (Calbiochem) at a detergent to protein ratio of 8:1 as described (70). Proteins (20 μg) were separated by BN-PAGE in 3–12% precast BN gels (Invitrogen).

To study the steady-state levels of the proteins, cortex samples were treated with Laemmli Sample Buffer (Bio-Rad), containing 5% β-mercaptoethanol. Proteins (20–40 μg) were separated by SDS–PAGE in 4–20% acrylamide gradient gels (Bio-Rad) and transferred onto PVDF membranes. Membranes were blocked with 5% non-fat dry milk in phosphate-buffered saline (PBS)–0.1% Tween 20 (PBST) and then blotted with specific primary antibodies. Secondary antibodies conjugated to horseradish peroxidase (Cell signaling) were used, and the reaction was developed by chemiluminescence using SuperSignal West reagent (Rockford, IL, USA).

Antibodies against NDUFA9, NDUFS3, NDUFS4, SDHA, UQCRC2, COXI, OXPHOS cocktail, Cytc, ETFA, MCAD, *N*-tyrosine, 4-HNE and voltage-dependent anion channel 1 were obtained from Abcam; Actin and Tubulin from Sigma; Tim 23 from BD Biosciences; SCOT from Santa Cruz Biotechnology; ACAT1 from Proteintech Group; GFAP from Cell Signaling; Tuj1 from Covance, SOD1 from Research Diagnostics; SOD2 from Upstate and polyclonal NDUFA5 antibody was donated by Dr John Walker (MRC, Cambridge, UK). All antibodies were used at 1/1000 dilution (in 0.15% milk in PBST), except for NDUFA5 used at 1/7500, ACAT1 used at 1/500, SCOT used at 1/100, *N*-tyrosine used at 1/400 and 4-HNE at 1/80 in blocking buffer (5% milk in PBST).

Enzymatic activity assays

Cortex homogenates were prepared in PBS containing complete protease inhibitor cocktail (Roche diagnostics) in a volume of 10× the weight. The tissue was disrupted by 10–15 strokes, using a motor-driven pestle. Homogenates were centrifuged at 100*g* for 5 min and supernatants used for enzymatic assays.

The activities of CI, CII, CIII and CIV and citrate synthase were measured spectrophotometrically as described (71). Protein concentrations were determined using the Bio-Rad Bradford Assay Kit with bovine serum albumin (BSA) as standard. Specific activity was determined and values represented as the percentage of control values performed simultaneously.

For fatty acid oxidation: activity of l-3-hydroxyacil-CoA dehydrogenase enzyme was assayed in reverse by measuring the decrease in absorbance at 340 nm due to the reduction of NADH using 30 μM acetoacetyl-CoA as described in refs (72,73). The activity of palmitoyl-CoA dehydrogenase was measured by determining the rate of dichlorophenol indophenol reduction by CoASH by a decrease in absorbance at 578 nm (73) using 40 μM palmitoyl-CoA as a substrate. The activities were normalized to protein concentration obtained by the Bradford method and expressed as μmol/min/mg of protein.

Lactate measurements

Blood was collected from the heart of anesthetized mice, centrifuged and lactate levels were measured in plasma in TAMU CVM Clinical Pathology Laboratory, TX, USA.

Immunohistochemistry

Anesthetized mice were transcardially perfused with ice-cold PBS, and half hemispheres were quickly isolated and fixed in 4% paraformaldehyde overnight and subsequently cryoprotected by incubation in 30% sucrose solution prepared in PBS. The cryoprotected brains were submerged in OCT Compound solution (TissueTek) and quickly frozen in 2-methylbutane cooled in liquid nitrogen. Sagittal sections were cut at a 30 μm thickness on a cryostat (Leica) and stored at −80°C before used.

For morphology analysis, 30 μm sections were prepared for a standard H&E staining. Images were captured with an Olympus BX51 microscope. Representative cerebral cortex and hippocampus areas of $n = 5$ per group are shown.

For the immunostaining of oxidized nucleic acids, sections were washed in PBS 1× first and then microwave-heated twice for 1 min in 10 mM sodium citrate buffer (pH 6.0). Sections were then permeabilized in 0.2% Triton X-100 for 30 min, and endogenous peroxidase activity was quenched by immersing sections in 100% methanol containing 0.3% H_2O_2 for 30 min. After blocking sections with 10% normal goat serum for 1 h at room temperature, sections were incubated with monoclonal antibody against 8-hydroxy-2′-deoxyguanosine (OH^8dG) and 8-hydroxyguanosine (OH^8G) (1:1000, QED Bioscience) for 2 h at 4°C in 5% goat serum. The bound primary antibody was detected as stated above using streptavidin peroxidase/DAB staining. For negative control, brain sections were pre-incubated with 10 μg/μl RNase (Qiagen) and 0.04 units/μl DNase (Promega) in 1× reaction buffer (Promega) for 1 h at 37°C prior to the primary antibody incubation. For positive control, brain sections were pre-treated with 30% H_2O_2 for 10 min before blocking with NGS. Images were captured with an Olympus BX51 microscope.

For fluorescent immunohistochemistry images, 30 μm sections were thawed at room temperature, washed in PBS and permeabilized with 0.4% Triton X-100 in PBS. Slides were blocked with 2% BSA for 1 h at room temperature and incubated with primary monoclonal antibody anti-NDUFA9 (1/200, Abcam), monoclonal anti-GFAP (1/200, Cell Signaling) and polyclonal anti-Iba1 (1/1000, Wako) overnight at 4°C. Specific Alexa 488- or 594-conjugated secondary antibody (1/500, Invitrogen) and the monoclonal antibody anti-COX1-Alex-488-conjugated (Abcam) were used for 3 h at room temperature in the dark. After washing, the slides were mounted with fluorescent mounting media containing 4′,6-diamidino-2-phenylindole (Vector Laboratories). Images were captured using an LSM710 confocal microscope (Zeiss). For the detection of cell death, tunel staining was performed following manufacturer' s instructions, using the TM *In Situ* Cell Death Detection Kit (Roche).

Quantification of the number of neurons was determined by counting the number of NeuN-positive cells in motor cortex and CA1 region. Thirty micrometer sections from control and *Ndufa5* CNS mice were stained for NeuN (1:200, Millipore) overnight at 4°C. The NeuN-bound antibody was detected with streptavidin peroxidase/DAB staining. After mounting, pictures were acquired with a Zeiss Axiovert 200M microscope. Neurons were quantified using the fractionator's probe, MBF Bioscience Stereo investigator 9.10.2. For motor cortex region, counting frame (C.F.) was 50 × 50 μ^2, and sample grid (S.G.) was 125 × 125 μ^2. For CA1 region, C.F. was 25 × 25 μ^2 and S.G. was 50 × 75 μ^2. ($n = 3$ for each group).

Statistical analysis

Data were analyzed using a two-tailed, unpaired Student's *t*-test between the two groups. Differences were considered significant when $P < 0.05$.

SUPPLEMENTARY MATERIAL

Supplementary Material is available at *HMG* online.

Conflict of Interest statement. None declared.

FUNDING

This work was supported by the National Institutes of Health (grants 1R01NS079965 and 1R01AG036871 to C.T.M. and 1R01GM101225 to F.D.), United Mitochondrial Disease Foundation to T.W. and the Muscular Dystrophy Association to C.T.M.

REFERENCES

1. Ugalde, C., Vogel, R., Huijbens, R., Van Den Heuvel, B., Smeitink, J. and Nijtmans, L. (2004) Human mitochondrial complex I assembles through the combination of evolutionary conserved modules: a framework to interpret complex I deficiencies. *Hum. Mol. Genet.*, **13**, 2461–2472.
2. Koopman, W.J., Nijtmans, L.G., Dieteren, C.E., Roestenberg, P., Valsecchi, F., Smeitink, J.A. and Willems, P.H. (2010) Mammalian mitochondrial

complex I: biogenesis, regulation, and reactive oxygen species generation. *Antioxid. Redox Signal.*, **12**, 1431–1470.
3. Carroll, J., Fearnley, I.M., Shannon, R.J., Hirst, J. and Walker, J.E. (2003) Analysis of the subunit composition of complex I from bovine heart mitochondria. *Mol. Cell. Proteomics*, **2**, 117–126.
4. Carroll, J., Fearnley, I.M., Skehel, J.M., Shannon, R.J., Hirst, J. and Walker, J.E. (2006) Bovine complex I is a complex of 45 different subunits. *J. Biol. Chem.*, **281**, 32724–33277.
5. Baradaran, R., Berrisford, J.M., Minhas, G.S. and Sazanov, L.A. (2013) Crystal structure of the entire respiratory complex I. *Nature*, **494**, 443–448.
6. Hunte, C., Zickermann, V. and Brandt, U. (2010) Functional modules and structural basis of conformational coupling in mitochondrial complex I. *Science*, **329**, 448–451.
7. Mimaki, M., Wang, X., McKenzie, M., Thorburn, D.R. and Ryan, M.T. (2012) Understanding mitochondrial complex I assembly in health and disease. *Biochim. Biophys. Acta*, **1817**, 851–862.
8. Schaefer, A.M., Taylor, R.W., Turnbull, D.M. and Chinnery, P.F. (2004) The epidemiology of mitochondrial disorders–past, present and future. *Biochim. Biophys. Acta*, **1659**, 115–120.
9. Pagniez-Mammeri, H., Loublier, S., Legrand, A., Benit, P., Rustin, P. and Slama, A. (2012) Mitochondrial complex I deficiency of nuclear origin I. Structural genes. *Mol. Genet. Metab.*, **105**, 163–172.
10. Diaz, F., Kotarsky, H., Fellman, V. and Moraes, C.T. (2011) Mitochondrial disorders caused by mutations in respiratory chain assembly factors. *Semin. Fetal Neonatal Med.*, **16**, 197–204.
11. Nouws, J., Nijtmans, L.G., Smeitink, J.A. and Vogel, R.O. (2012) Assembly factors as a new class of disease genes for mitochondrial complex I deficiency: cause, pathology and treatment options. *Brain*, **135**, 12–22.
12. Pagniez-Mammeri, H., Rak, M., Legrand, A., Benit, P., Rustin, P. and Slama, A. (2012) Mitochondrial complex I deficiency of nuclear origin II. Non-structural genes. *Mol. Genet. Metab.*, **105**, 173–179.
13. Orth, M. and Schapira, A.H. (2001) Mitochondria and degenerative disorders. *Am. J. Med. Genet.*, **106**, 27–36.
14. Parker, W.D. Jr, Boyson, S.J., Luder, A.S. and Parks, J.K. (1990) Evidence for a defect in NADH: ubiquinone oxidoreductase (complex I) in Huntington's disease. *Neurology*, **40**, 1231–1234.
15. Parker, W.D. Jr and Parks, J.K. (2005) Mitochondrial ND5 mutations in idiopathic Parkinson's disease. *Biochem. Biophys. Res. Commun.*, **326**, 667–669.
16. Smigrodzki, R., Parks, J. and Parker, W.D. (2004) High frequency of mitochondrial complex I mutations in Parkinson's disease and aging. *Neurobiol. Aging*, **25**, 1273–1281.
17. Betarbet, R., Sherer, T.B., MacKenzie, G., Garcia-Osuna, M., Panov, A.V. and Greenamyre, J.T. (2000) Chronic systemic pesticide exposure reproduces features of Parkinson's disease. *Nat. Neurosci.*, **3**, 1301–1306.
18. Cannon, J.R. and Greenamyre, J.T. (2010) Neurotoxic in vivo models of Parkinson's disease recent advances. *Prog. Brain Res.*, **184**, 17–33.
19. Dawson, T.M. and Dawson, V.L. (2003) Molecular pathways of neurodegeneration in Parkinson's disease. *Science*, **302**, 819–822.
20. Fornai, F., Schluter, O.M., Lenzi, P., Gesi, M., Ruffoli, R., Ferrucci, M., Lazzeri, G., Busceti, C.L., Pontarelli, F., Battaglia, G. *et al.* (2005) Parkinson-like syndrome induced by continuous MPTP infusion: convergent roles of the ubiquitin-proteasome system and alpha-synuclein. *Proc. Natl. Acad. Sci. USA*, **102**, 3413–3418.
21. Lin, M.T. and Beal, M.F. (2006) Mitochondrial dysfunction and oxidative stress in neurodegenerative diseases. *Nature*, **443**, 787–795.
22. Koene, S., Willems, P.H., Roestenberg, P., Koopman, W.J. and Smeitink, J.A. (2011) Mouse models for nuclear DNA-encoded mitochondrial complex I deficiency. *J. Inherit. Metab. Dis.*, **34**, 293–307.
23. Ingraham, C.A., Burwell, L.S., Skalska, J., Brookes, P.S., Howell, R.L., Sheu, S.S. and Pinkert, C.A. (2009) NDUFS4: creation of a mouse model mimicking a Complex I disorder. *Mitochondrion*, **9**, 204–210.
24. Kruse, S.E., Watt, W.C., Marcinek, D.J., Kapur, R.P., Schenkman, K.A. and Palmiter, R.D. (2008) Mice with mitochondrial complex I deficiency develop a fatal encephalomyopathy. *Cell Metab.*, **7**, 312–320.
25. Leong, D.W., Komen, J.C., Hewitt, C.A., Arnaud, E., McKenzie, M., Phipson, B., Bahlo, M., Laskowski, A., Kinkel, S.A., Davey, G.M. *et al.* (2012) Proteomic and metabolomic analyses of mitochondrial complex I-deficient mouse model generated by spontaneous B2 short interspersed nuclear element (SINE) insertion into NADH dehydrogenase (ubiquinone) Fe-S protein 4 (Ndufs4) gene. *J. Biol. Chem.*, **287**, 20652–20663.
26. Quintana, A., Kruse, S.E., Kapur, R.P., Sanz, E. and Palmiter, R.D. (2010) Complex I deficiency due to loss of Ndufs4 in the brain results in progressive encephalopathy resembling Leigh syndrome. *Proc. Natl. Acad. Sci. USA.*, **107**, 10996–11001.
27. Quintana, A., Zanella, S., Koch, H., Kruse, S.E., Lee, D., Ramirez, J.M. and Palmiter, R.D. (2012) Fatal breathing dysfunction in a mouse model of Leigh syndrome. *J. Clin. Invest.*, **122**, 2359–2368.
28. Ke, B.X., Pepe, S., Grubb, D.R., Komen, J.C., Laskowski, A., Rodda, F.A., Hardman, B.M., Pitt, J.J., Ryan, M.T., Lazarou, M. *et al.* (2012) Tissue-specific splicing of an Ndufs6 gene-trap insertion generates a mitochondrial complex I deficiency-specific cardiomyopathy. *Proc. Natl. Acad. Sci. USA.*, **109**, 6165–6170.
29. Klein, J.A., Longo-Guess, C.M., Rossmann, M.P., Seburn, K.L., Hurd, R.E., Frankel, W.N., Bronson, R.T. and Ackerman, S.L. (2002) The harlequin mouse mutation downregulates apoptosis-inducing factor. *Nature*, **419**, 367–374.
30. Vahsen, N., Cande, C., Briere, J.J., Benit, P., Joza, N., Larochette, N., Mastroberardino, P.G., Pequignot, M.O., Casares, N., Lazar, V. *et al.* (2004) AIF deficiency compromises oxidative phosphorylation. *EMBO J.*, **23**, 4679–4689.
31. Lin, C.S., Sharpley, M.S., Fan, W., Waymire, K.G., Sadun, A.A., Carelli, V., Ross-Cisneros, F.N., Baciu, P., Sung, E., McManus, M.J. *et al.* (2012) Mouse mtDNA mutant model of Leber hereditary optic neuropathy. *Proc. Natl. Acad. Sci. USA.*, **109**, 20065–20070.
32. Carroll, J., Shannon, R.J., Fearnley, I.M., Walker, J.E. and Hirst, J. (2002) Definition of the nuclear encoded protein composition of bovine heart mitochondrial complex I. Identification of two new subunits. *J. Biol. Chem.*, **277**, 50311–50317.
33. Stanford, W.L., Cohn, J.B. and Cordes, S.P. (2001) Gene-trap mutagenesis: past, present and beyond. *Nat. Rev. Genet.*, **2**, 756–768.
34. Dragatsis, I. and Zeitlin, S. (2000) CaMKIIalpha-Cre transgene expression and recombination patterns in the mouse brain. *Genesis*, **26**, 133–135.
35. DeBerardinis, R.J., Lum, J.J., Hatzivassiliou, G. and Thompson, C.B. (2008) The biology of cancer: metabolic reprogramming fuels cell growth and proliferation. *Cell Metab.*, **7**, 11–20.
36. DiMauro, S. and Schon, E.A. (2008) Mitochondrial disorders in the nervous system. *Annu. Rev. Neurosci.*, **31**, 91–123.
37. Tieu, K., Perier, C., Caspersen, C., Teismann, P., Wu, D.C., Yan, S.D., Naini, A., Vila, M., Jackson-Lewis, V., Ramasamy, R. *et al.* (2003) D-beta-hydroxybutyrate rescues mitochondrial respiration and mitigates features of Parkinson disease. *J. Clin. Invest.*, **112**, 892–901.
38. Distelmaier, F., Koopman, W.J., van den Heuvel, L.P., Rodenburg, R.J., Mayatepek, E., Willems, P.H. and Smeitink, J.A. (2009) Mitochondrial complex I deficiency: from organelle dysfunction to clinical disease. *Brain*, **132**, 833–842.
39. Kasai, H., Tanooka, H. and Nishimura, S. (1984) Formation of 8-hydroxyguanine residues in DNA by X-irradiation. *Gann*, **75**, 1037–1039.
40. Acin-Perez, R., Fernandez-Silva, P., Peleato, M.L., Perez-Martos, A. and Enriquez, J.A. (2008) Respiratory active mitochondrial supercomplexes. *Mol. Cell.*, **32**, 529–539.
41. Schagger, H. and Pfeiffer, K. (2000) Supercomplexes in the respiratory chains of yeast and mammalian mitochondria. *EMBO J.*, **19**, 1777–1783.
42. Diaz, F., Garcia, S., Padgett, K.R. and Moraes, C.T. (2012) A defect in the mitochondrial complex III, but not complex IV, triggers early ROS-dependent damage in defined brain regions. *Hum. Mol. Genet.*, **21**, 5066–5077.
43. Fukui, H., Diaz, F., Garcia, S. and Moraes, C.T. (2007) Cytochrome c oxidase deficiency in neurons decreases both oxidative stress and amyloid formation in a mouse model of Alzheimer's disease. *Proc. Natl. Acad. Sci. USA.*, **104**, 14163–14168.
44. Watmough, N.J. and Frerman, F.E. (2010) The electron transfer flavoprotein: ubiquinone oxidoreductases. *Biochim. Biophys. Acta*, **1797**, 1910–1916.
45. Baranano, K.W. and Hartman, A.L. (2008) The ketogenic diet: uses in epilepsy and other neurologic illnesses. *Curr. Treat. Options Neurol.*, **10**, 410–419.
46. Guzman, M. and Blazquez, C. (2004) Ketone body synthesis in the brain: possible neuroprotective effects. *Prostaglandins Leukot. Essent. Fatty Acids*, **70**, 287–292.
47. Jonas, R. and Huth, W. (1978) Acetyl-CoA acetyltransferase from bovine liver mitochondria. Molecular properties of multiple forms. *Biochim. Biophys. Acta*, **527**, 379–390.
48. Wenz, T., Luca, C., Torraco, A. and Moraes, C.T. (2009) mTERF2 regulates oxidative phosphorylation by modulating mtDNA transcription. *Cell Metab.*, **9**, 499–511.

49. Ahola-Erkkila, S., Carroll, C.J., Peltola-Mjosund, K., Tulkki, V., Mattila, I., Seppanen-Laakso, T., Oresic, M., Tyynismaa, H. and Suomalainen, A. (2010) Ketogenic diet slows down mitochondrial myopathy progression in mice. *Hum. Mol. Genet.*, **19**, 1974–1984.
50. Yao, J., Chen, S., Mao, Z., Cadenas, E. and Brinton, R.D. (2011) 2-Deoxy-d-glucose treatment induces ketogenesis, sustains mitochondrial function, and reduces pathology in female mouse model of Alzheimer's disease. *PLoS One*, **6**, e21788.
51. Huth, W. (1981) The charge heterogeneity of the mitochondrial acetyl-CoA acetyltransferase from rat liver. *Eur. J. Biochem.*, **120**, 557–562.
52. Blazquez, C., Sanchez, C., Velasco, G. and Guzman, M. (1998) Role of carnitine palmitoyltransferase I in the control of ketogenesis in primary cultures of rat astrocytes. *J. Neurochem.*, **71**, 1597–1606.
53. Edmond, J., Robbins, R.A., Bergstrom, J.D., Cole, R.A. and de Vellis, J. (1987) Capacity for substrate utilization in oxidative metabolism by neurons, astrocytes, and oligodendrocytes from developing brain in primary culture. *J. Neurosci. Res.*, **18**, 551–561.
54. Morris, A.A. (2005) Cerebral ketone body metabolism. *J. Inherit. Metab. Dis.*, **28**, 109–121.
55. Chinopoulos, C. (2013) Which way does the citric acid cycle turn during hypoxia? The critical role of alpha-ketoglutarate dehydrogenase complex. *J. Neurosci. Res.*, **91**, 1030–1043.
56. Weinberg, J.M., Venkatachalam, M.A., Roeser, N.F. and Nissim, I. (2000) Mitochondrial dysfunction during hypoxia/reoxygenation and its correction by anaerobic metabolism of citric acid cycle intermediates. *Proc. Natl. Acad. Sci. USA.*, **97**, 2826–2831.
57. Koopman, W.J., Verkaart, S., Visch, H.J., van der Westhuizen, F.H., Murphy, M.P., van den Heuvel, L.W., Smeitink, J.A. and Willems, P.H. (2005) Inhibition of complex I of the electron transport chain causes $O^{2-\cdot}$-mediated mitochondrial outgrowth. *Am. J. Physiol. Cell Physiol.*, **288**, C1440–C1450.
58. Verkaart, S., Koopman, W.J., van Emst-de Vries, S.E., Nijtmans, L.G., van den Heuvel, L.W., Smeitink, J.A. and Willems, P.H. (2007) Superoxide production is inversely related to complex I activity in inherited complex I deficiency. *Biochim. Biophys. Acta*, **1772**, 373–381.
59. Murphy, M.P. (2009) How mitochondria produce reactive oxygen species. *Biochem. J.*, **417**, 1–13.
60. Pinto, M., Pickrell, A.M., Fukui, H. and Moraes, C.T. (2013) Mitochondrial DNA damage in a mouse model of Alzheimer's disease decreases amyloid beta plaque formation. *Neurobiol. Aging*, **34**, 2399–2407.
61. Kujoth, G.C., Hiona, A., Pugh, T.D., Someya, S., Panzer, K., Wohlgemuth, S.E., Hofer, T., Seo, A.Y., Sullivan, R., Jobling, W.A. *et al.* (2005) Mitochondrial DNA mutations, oxidative stress, and apoptosis in mammalian aging. *Science*, **309**, 481–484.
62. Trifunovic, A., Hansson, A., Wredenberg, A., Rovio, A.T., Dufour, E., Khvorostov, I., Spelbrink, J.N., Wibom, R., Jacobs, H.T. and Larsson, N.G. (2005) Somatic mtDNA mutations cause aging phenotypes without affecting reactive oxygen species production. *Proc. Natl. Acad. Sci. USA.*, **102**, 17993–17998.
63. Hiona, A., Sanz, A., Kujoth, G.C., Pamplona, R., Seo, A.Y., Hofer, T., Someya, S., Miyakawa, T., Nakayama, C., Samhan-Arias, A.K. *et al.*. (2010) Mitochondrial DNA mutations induce mitochondrial dysfunction, apoptosis and sarcopenia in skeletal muscle of mitochondrial DNA mutator mice. *PLoS One*, **5**, e11468.
64. Iuso, A., Scacco, S., Piccoli, C., Bellomo, F., Petruzzella, V., Trentadue, R., Minuto, M., Ripoli, M., Capitanio, N., Zeviani, M. *et al.* (2006) Dysfunctions of cellular oxidative metabolism in patients with mutations in the NDUFS1 and NDUFS4 genes of complex I. *J. Biol. Chem.*, **281**, 10374–10380.
65. Huang, G., Chen, Y., Lu, H. and Cao, X. (2007) Coupling mitochondrial respiratory chain to cell death: an essential role of mitochondrial complex I in the interferon-beta and retinoic acid-induced cancer cell death. *Cell Death Differ.*, **14**, 327–337.
66. Kaminski, M., Kiessling, M., Suss, D., Krammer, P.H. and Gulow, K. (2007) Novel role for mitochondria: protein kinase Ctheta-dependent oxidative signaling organelles in activation-induced T-cell death. *Mol. Cell Biol.*, **27**, 3625–3639.
67. Fukui, H. and Moraes, C.T. (2008) The mitochondrial impairment, oxidative stress and neurodegeneration connection: reality or just an attractive hypothesis? *Trends Neurosci.*, **31**, 251–256.
68. Calvaruso, M.A., Smeitink, J. and Nijtmans, L. (2008) Electrophoresis techniques to investigate defects in oxidative phosphorylation. *Methods*, **46**, 281–287.
69. Diaz, F., Barrientos, A. and Fontanesi, F. (2009) Evaluation of the mitochondrial respiratory chain and oxidative phosphorylation system using blue native gel electrophoresis. *Curr. Protoc. Hum. Genet.*, Chapter 19, Unit 19 4.
70. Diaz, F., Fukui, H., Garcia, S. and Moraes, C.T. (2006) Cytochrome c oxidase is required for the assembly/stability of respiratory complex I in mouse fibroblasts. *Mol. Cell Biol.*, **26**, 4872–4881.
71. Barrientos, A., Fontanesi, F. and Diaz, F. (2009) Evaluation of the mitochondrial respiratory chain and oxidative phosphorylation system using polarography and spectrophotometric enzyme assays. *Curr. Protoc. Hum. Genet.*, Chapter 19, Unit 19 3.
72. Agrawal, V.P. and Kolattukudy, P.E. (1978) Mechanism of action of a wound-induced omega-hydroxyfatty acid:NADP oxidoreductase isolated from potato tubers (*Solanum tuberosum* L). *Arch. Biochem. Biophys.*, **191**, 466–478.
73. Srere, P.A., Seubert, W. and Lynen, F. (1959) Palmityl coenzyme A deacylase. *Biochim. Biophys. Acta*, **33**, 313–319.